ADVANCED ENERGY MATERIALS
www.advenergymat.de

Correlating the Photoshunt with Charge-Collection Losses in Organic Solar Cells

Eunchi Kim, Leonard Christen, and Thomas Kirchartz**

The low charge carrier mobility of molecular materials is one of the key obstacles to achieving higher efficiencies in organic photovoltaics. Therefore, understanding and quantifying charge collection losses owing to low mobility is an important challenge in organic photovoltaics and other emerging photovoltaic technologies. Here, an approach is proposed to use the photoshunt and its dependence on light intensity as an easily accessible indicator of charge-collection losses. The physical meaning of the photoshunt is explored using drift-diffusion simulations and an analytical model. The results show that the recombination current visible as the photoshunt is decreasing with increasing charge carrier mobility. Furthermore, a framework is presented for evaluating the short-circuit current losses in experimental data using a photoshunt. The study reveals that the charge-collection efficiency at shortcircuit is strongly influenced by the charge carrier mobility and light intensity.

1. Introduction

While the efficiencies of organic solar cells are continuously improving to values beyond 19%,[1–5] their performance is still lagging behind other state-of-the-art solar cells such as crystalline Si cells or perovskite cells.[6–8] To further improve efficiency, it is important to understand the origin of power losses. One detrimental factor is that blends of organic semiconductors have low charge carrier mobilities.[9–12] Charge carriers in the organic layer travel by hopping through the conjugated π-bonding along the backbone of the polymer or small molecule and therefore travel with orders of magnitude lower mobility than typical for inorganic semiconductors.[10,13,14] A consequence of this inefficient charge transport is that under steady-state illumination, a non-zero density of electrons and holes exists within the absorber layer also at shortcircuit and a significant recombination rate may be present. As recombination losses during charge extraction are difficult to disentangle from optical losses or resistive losses, the research community either focuses on oversimplified approaches such as the study of the linearity of the short-circuit current with light intensity[15–25], or uses sophisticated methods such as time-delayed collection field[26–29] measurements that require experimental equipment that is not available in all research groups.

Here, we study the use of the apparent photoshunt $R_{\mathrm{p,photo}}$ as a quantitative measure of charge collection losses within the context of organic photovoltaics using experiments, numerical simulations, and analytical modeling. The apparent photoshunt is a consequence of finite mobilities leading to deviations from the idealized superposition principle that is typically used to explain the difference between dark and illuminated current-voltage curves.[30] The current-voltage curve of an illuminated solar cell according to the so-called superposition principle is described as $J(V) = J_{\mathrm{d}} - J_{\mathrm{sc}}$, i.e., the dark current density $J_{\mathrm{d}}(V)$, which depends on the voltage V, minus the voltage-independent short-circuit current density J_{sc}.

Therefore, in this work, we demonstrate how the photoshunt depends on mobility and light intensity. Moreover, because the photoshunt is inversely proportional to the light intensity ϕ to a good approximation, we introduce a new figure of merit (FOM), namely the product $R_{\mathrm{p,photo}}\phi$, which is expected to show a distinct dependence on a material parameter such as mobility μ. Thus, we use it to understand the charge extraction loss at short-circuit in organic solar cells. To interpret the charge collection behavior of organic solar cells more accurately, we analyzed $R_{\mathrm{p,photo}}\phi$ with two other assays for charge extraction efficiency–the fill factor FF and the charge-collection efficiency at $V = 0$ V. Based on the drift-diffusion simulation, we analyze the experimental data using a combination of varied process parameters and light intensity and introduce a novel analytical framework for utilizing the three FOMs for quantifying short-circuit current losses.

2. Results and Discussion

To verify the universality of our observations, we present the experimental data of light-intensity-dependent J–V

E. Kim, L. Christen, T. Kirchartz
IMD-3 Photovoltaik
Forschungszentrum Jülich
52425 Jülich, Germany
E-mail: e.kim@fz-juelich.de; t.kirchartz@fz-juelich.de
T. Kirchartz
Faculty of Engineering and CENIDE
University of Duisburg-Essen
Carl-Benz-Str. 199, 47057 Duisburg, Germany

The ORCID identification number(s) for the author(s) of this article can be found under https://doi.org/10.1002/aenm.202403129

DOI: 10.1002/aenm.202403129

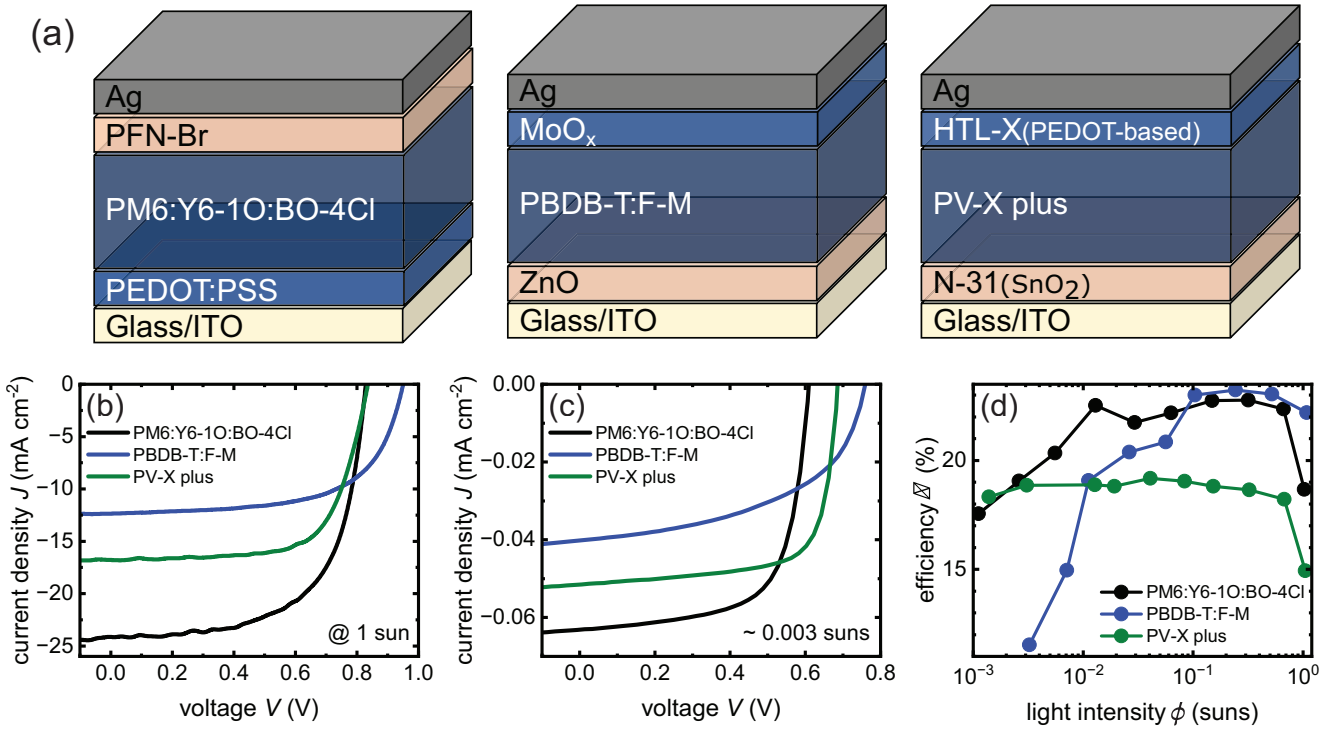

Figure 1. a) Schematics of different solar cell architectures used in this study. b) The $J-V$ curves measured under AM1.5G illumination and c) under white LED illumination (≈0.003 suns). d) Efficiency as a function of light intensity measured with LED lamp. The spectral irradiance of the white LED was used to correct its power density.[35]

measurements on organic solar cells with three different stacks and donor: acceptor blends (**Figure** 1a). The full names and chemical structures can be found in the Methods section of the Supporting Information. We selected PM6:Y6-1O:BO-4Cl, PBDB-T:F-M, and PV-X plus as the absorbing molecular materials for the photoactive layer, as they are promising candidates for exhibiting a good performance in the environmentally friendly solvent *o*-xylene. The PM6:Y6-1O:BO-4Cl showed an efficiency of 18.3% under AM 1.5G conditions, which is the highest reported value for the *o*-xylene-based active layer, to the best of our knowledge.[31] The PBDB-T:F-M has been utilized in tandem solar cells, attributed to its high band gap[32] and compatibility with *o*-xylene.[33] PV-X plus is a commercial absorber layer blend processed in *o*-xylene and is expected to facilitate upscaling and industrial applications. However, the specific materials comprising the blend, apart from $PC_{61}BM$, have not been disclosed.[34]

Figure 1b displays $J-V$ curves measured under AM1.5G illumination of the cell with the respective active layer, while Figure 1c,d illustrate the results of white LED $J-V$ measurements at varied light intensity. Note that the efficiency measured under LED lamp is higher than that obtained under standard solar spectrum. (see Tables S2 and S3, Supporting Information) This deviation arises from the spectral properties of the LED, which has a narrower emission peak within the 400–700 nm range. As the light intensity decreases from 1 sun (Figure 1b) to ≈ 0.003 suns (Figure 1c), the overall performance of the solar cell changes accordingly. At low light intensity, the efficiency is limited primarily by the reduced V_{oc}, since J_{sc} scales approximately with the light intensity ϕ. As shown in Figure 1d, the PBDB-T:F-M cell experiences a drastic drop in efficiency toward lower light intensities. This drop is caused by the dark shunt resistance $R_{p,dark}$ of 15 kΩ cm^2, which is significantly lower than that of the PM6:Y6-1O:BO-4Cl (1200 kΩ cm^2) and PV-X plus (102 kΩ cm^2) cells. As the light intensity increases, the efficiency of the solar cell increases until it reaches a maximum point, after which it declines. Voltage drops with the magnitude $\Delta V = JR_s$ due to series resistance R_s result in increasing efficiency losses at higher light intensities.

With the $J-V$ curves plotted in the fourth quadrant as seen in Figure 1b,c, it is still difficult to compare their characteristics, since the current density differs by orders of magnitude. To address this issue, plotting shifted $J-V$ curves, that is the sum $J(V) + J_{sc}$, on a logarithmic scale against voltage is often employed.[30,33,36,37] This approach enables us not only to better visualize the voltage-dependent recombination currents for various light intensities but also unveils the presence of a shunt resistance under illumination that differs from the dark shunt. Accordingly, **Figure** 2 displays the shifted $J-V$ curves of the PM6:Y6-1O:BO-4Cl, PBDB-T:F-M, and PV-X plus solar cell at varied light intensity. These plots resemble the dark $J-V$ curves insofar as it seems that the current is limited by the shunt resistance at low voltages. The current in this region increases with the light intensity, indicating a decrease in the shunt resistance. Moreover, when the shifted $J-V$ curve is plotted on a double-logarithmic scale, it reveals an ohmic behavior at low voltages where current densities scale nearly linearly with the voltage (see Figure S3, Supporting Information). The observation of light-intensity-dependent apparent shunt resistance is a

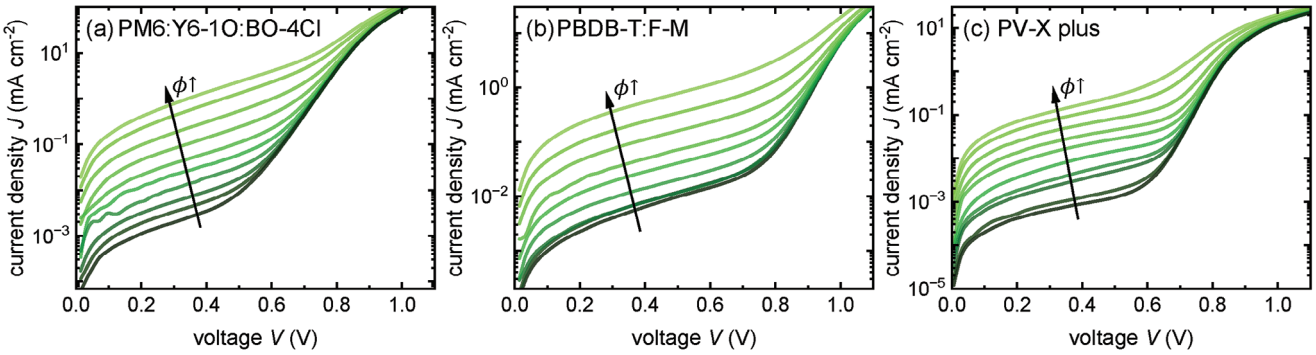

Figure 2. Measurements showing shifted $J-V$ curves $J(V)+J_{sc}$ of organic solar cells with the active layer blends a) PM6:Y6-1O:BO-4Cl, b) PBDB-T:F-M, and c) PV-X plus. In all cases, the approximately ohmic current flowing at low forward bias increases significantly with light intensity indicating that there exists an effective light-intensity dependent shunt resistance.

general feature of solar cells that originates from recombination of photogenerated but uncollected charge carriers whose concentration depends primarily on the mobility of the charge carriers. This recombination current of photogenerated carriers exhibits a weak or even linear dependence on the external voltage.[36] In organic solar cells, a linear voltage-dependent recombination current could in principle be due to geminate[38–40] or non-geminate recombination, whereby we will focus in our simulations on the latter possibility. Since non-geminate recombination depends exponentially on the Fermi level splitting ΔE_F, it may appear counterintuitive that it leads to a quasi-ohmic behavior. However, this effect can be rationalized by the weak dependence of quasi-Fermi-level splitting. ΔE_F on the external voltage under illumination and low forward voltages.[41] As long as the change in ΔE_F according to the external voltage is only slightly more than k_BT, the additional recombination current caused by the increase in ΔE_F would only cause a linear increase in current. Mathematically saying, we can Taylor-expand (note $e^x - 1 \approx x$, when $x \to 0$) the shift current J_{shift} in the following way

$$J_{shift} \propto \exp\left(\frac{\Delta E_F(V) - \Delta E_F(0)}{n_{id}k_BT}\right) - 1 \approx \frac{\Delta E_F(V) - \Delta E_F(0)}{n_{id}k_BT} \quad (1)$$

provided that $\Delta E_F(V) - \Delta E_F(0) \ll n_{id}k_BT$ is holding true.[36] Thus, if ΔE_F changes only slightly with voltage, every exponential recombination current may appear linear with respect to the change $\Delta E_F(V) - \Delta E_F(0)$ in the Fermi-level splitting. In addition, the value $\Delta E_F(V) - \Delta E_F(0)$ will change not only weakly but also approximately linearly with external voltage V. In the voltage range where both of these conditions are fulfilled to a good approximation, the shift current would exhibit an ohmic behavior, thereby causing the apparent photoshunt to become visible both in simulations and in experiments.

In the following section, we discuss how mobilities and light intensity influence $R_{p,photo}$. **Figure 3** displays $J-V$ and shifted $J-V$ curves of an illuminated solar cell with varied mobility and light intensity, based on the drift-diffusion simulation results. The FF and J_{sc} improve with charge carrier mobility (Figure 3a). Once the mobility exceeds $\approx 10^{-1}$ cm^2 V^{-1} s^{-1}, the FF saturates at ≈85% and the $J-V$ curves overlap, making it difficult to evaluate their charge transport properties. However, shifted $J-V$ curves plotted in the first quadrant allow us the intuitive comparison of the $R_{p,photo}$ across different mobilities (Figure 3b). In general, $R_{p,photo}$ increases with the mobility, indicating more electrons are extracted at the contact before recombination. However, as the mobility decreases below a certain threshold ($<10^{-4}$ cm^2 V^{-1} s^{-1}), $R_{p,photo}$ reaches a minimum and is increasing toward even lower mobilities. This is because of the influence of low mobilities on the series resistance of the solar cell. Once the series resistance increases such that it approaches the shunt resistance, the $J-V$ curve becomes nearly entirely ohmic and further reductions in mobility then result in higher series resistances. This would also be interpreted as a higher shunt resistance as the two resistances become indistinguishable (Figure 3a). Hence, $R_{p,photo}$ rather increases despite decreasing charge carrier mobility, as indicated by the arrow in Figure 3b. Additionally, we examined the light-intensity-dependent performance of an organic solar cell based on the simulation results. When the light intensity increases from 10^{-3} to 1 sun, J_{sc} and V_{oc} increase since both terms are related to the charge carrier density. However, the gradual increase in the shifted $J-V$ curves with increasing light intensity suggests a decline in charge-extraction efficiency. In summary, $R_{p,photo}$, which indicates how good the charge extraction is, is influenced by the charge carrier mobility and the light intensity.

To analyze the photoshunt of the cells that we produce in our laboratory, we need to consider that solar cells inevitably suffer from a finite dark shunt resistance $R_{p,dark}$. The $R_{p,total}$, which is the inverse slope of illuminated $J-V$ curves dJ/dV at $V = 0$, inherently contains the information of both $R_{p,photo}$ and $R_{p,dark}$ and, therefore, the extraction of $R_{p,photo}$ from the $R_{p,total}$ is a mandatory step prior to analysis. In **Figure 4a,b**, the simulated and experimental photoshunt resistances $R_{p,photo}$ (squares) and total shunt resistance $R_{p,total}$ (circles) are plotted versus the light intensity on a double-logarithmic plot, respectively. At low light intensity, the simulation results of $R_{p,total}$ saturates at 100 kΩ cm^2, which is the value $R_{p,dark}$ is originally set at (Figure 4a). Based on this observation, we assume the $R_{p,total}$ at the light intensity below 10^{-3} suns is equal to $R_{p,dark}$, using it to correct $R_{p,total}$ at higher light intensity. Once $R_{p,total}$ is corrected according to $1/R_{p,photo} = 1/R_{p,total} - 1/R_{p,dark}$, the $R_{p,photo}$ displays the proportionality to the inverse of light intensity $1/\phi$ (Figure 4a). Now, we examine how the corrected $R_{p,photo}$ evolves with the irradiance in real solar cells. The results of the solar cells with the corresponding active layer are displayed in Figure 4b. Similar to the simulation

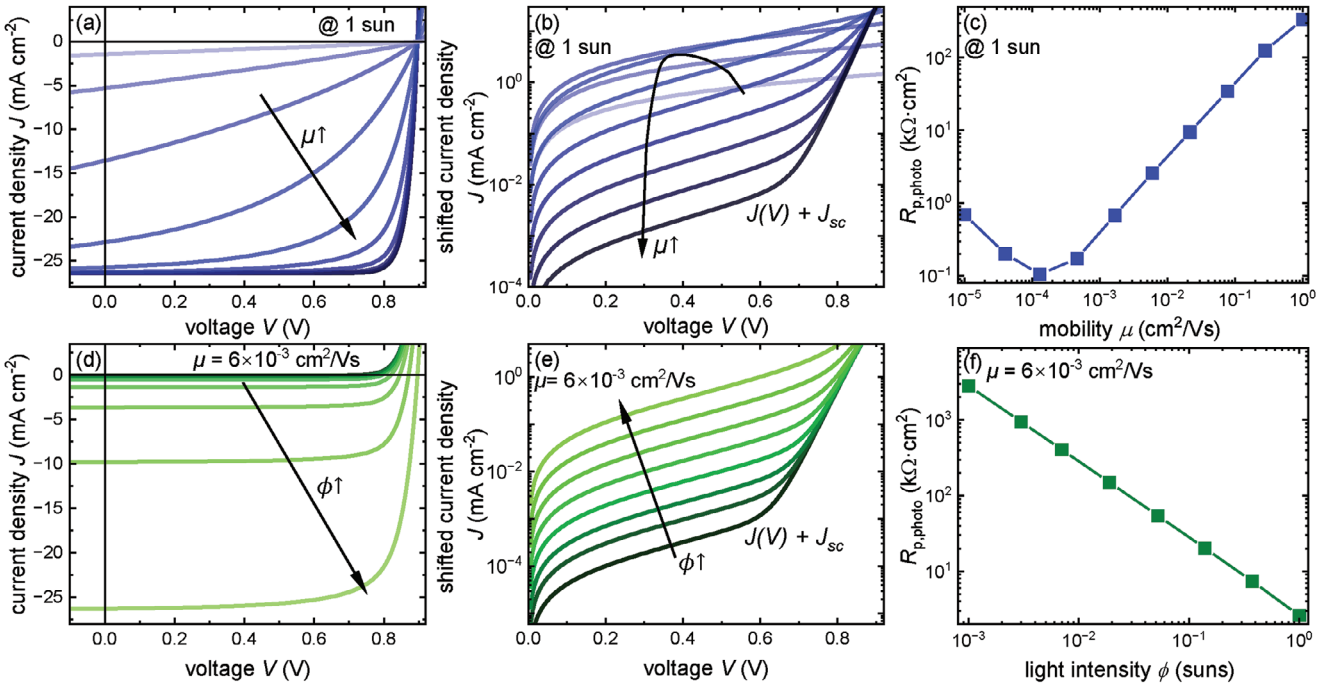

Figure 3. a,d) Simulated J–V curves and b,e) shifted J–V curves $J(V) + J_{sc}$ of varied charge carrier mobility μ ($10^{-5} \sim 1$ cm^2 V^{-1} s^{-1}) at a fixed light intensity of 1 sun (a,b) and of varied light intensity (0.001 ~ 1 sun) at a fixed charge carrier mobility of 6×10^{-3} cm^2 V^{-1} s^{-1} d,e). c,f) Photoshunt as a function of mobility c) and light intensity f).

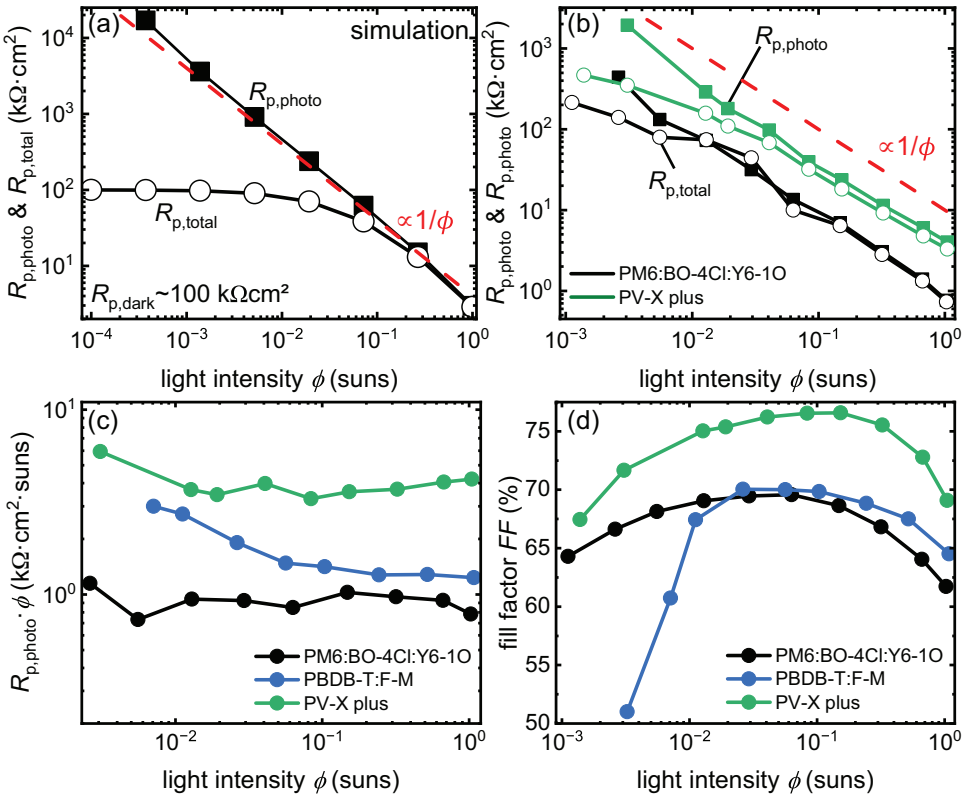

Figure 4. The photoshunt $R_{p,photo}$ (squares) and the total shunt resistance $R_{p,total}$ (circles) of a) simulated and b) measured illuminated J–V characteristics with different light intensities on a double-logarithmic scale. The corresponding c) $R_{p,photo}\phi$ and d) FF are plotted against light intensity. The $R_{p,total}$ saturates to the value of $R_{p,dark}$ with decreasing light intensity, whereas the corrected $R_{p,photo}$ does not.

results, the extracted $R_{p,photo}$ of the different cell stacks as a function of light intensity is almost parallel to the red dashed line representing ϕ^{-1}, implying the importance of the correction in advance to the data interpretation and the generality of our observations. (The results of the PBDB-T:F-M cell can be found in Figure S5, Supporting Information.) The proportional relationship between $R_{p,photo}$ and ϕ^{-1} is linked to how the recombination rate R scales with the light intensity. The $R_{p,photo}$ reflects the voltage-dependence of the photocurrent ΔJ_{ph} and the photocurrents indicate the generation and recombination of the charges, where $J_{ph} = q\int_0^d (G(\phi, V, x) - R(\phi, V, x))dx$. Since the generation rate G is proportional to ϕ, $R_{p,photo}\phi$ will remain constant as long as the recombination scales linearly with the light intensity. However, the simulation presented in this paper solely considers direct recombination, that is, the recombination rate scales with the product of photogenerated electron(n) and hole(p) densities ($R \propto np$). As highlighted in a previous study,[42] direct or bimolecular recombination can scale linearly or quadratic with light intensity. This finding may initially appear counterintuitive as the distinguishing feature of direct recombination that the recombination rate scales with the np-product. Furthermore, in an intrinsic semiconductor at short-circuit, the average density of electrons and the average density of holes each scale linearly with light intensity. The key to understand direct recombination that scales linearly with light intensity is to acknowledge the fact that both carrier densities and, in consequence, recombination rates can be a strong function of depth in the absorber layer. At lower light intensities, for instance, the densities of injected electrons close to the cathode would significantly exceed the density of photogenerated electrons and holes (close to the cathode). Therefore, the recombination rate would scale linearly with hole density and linearly with the injected electron density that is however mostly independent of light intensity. The opposite would be true close to the anode, where it is the injected hole density and the photogenerated electron density whose product scales linearly with light intensity. Only in the middle of the device, far away from either cathode or anode, the recombination rate may scale with the square of the light intensity. As one can see in Figure S4 (Supporting Information), the influence of the contact-injected charge carriers dominates the overall recombination rate especially at lower light intensities, and might still be dominant at one sun. Thus, direct recombination may lead to a scaling of the overall recombination rate that is linear with light intensity, thereby not affecting the linearity of J_{sc} and ϕ. It is intuitive to assume that the same is valid for the inverse proportionality of $R_{p,photo}$ and ϕ. Within the framework of the model derived by Sandberg and Armin,[43] it is possible to derive that the conditions that cause $J_{sc} \propto \phi$ to be valid are mathematically identical to the conditions that cause $R_{p,photo} \propto 1/\phi$ to be valid (see Supporting Information, Note 2, Supporting Information). Thus, the common overinterpretation[15–25] of the experimental finding that $J_{sc} \propto \phi$ is valid as being indicative of an absence of any (strong) bimolecular recombination at short circuit and is equally relevant for the interpretation of the relation $R_{p,photo} \propto 1/\phi$ being valid. However, the big advantage of studying the photoshunt is that the absolute value $R_{p,photo}\phi$ contains information that cannot be accessed by studying the light-intensity dependence of J_{sc}.

The strong relationship between $R_{p,photo}$ and ϕ instigates us to investigate $R_{p,photo}\phi$ as a new observable in J–V curves. In Figure 4c, $R_{p,photo}\phi$ of the three different cells remains relatively constant over light intensity to a good approximation. The comparison between Figure 4c,d suggests a possible correlation between $R_{p,photo}\phi$ and FF. Therefore, we propose that $R_{p,photo}\phi$ is a new figure of merit for evaluating charge extraction efficiency and providing insights into the physics of charge collection while only requiring simple characterization and data analysis methods. As mentioned in the previous section, due to the notably low $R_{p,dark}$ observed in the PBDB-T:F-M cell, FF undergoes a substantial decrease at low light intensities.

Therefore, in order to understand the physical significance of $R_{p,photo}\phi$, we endeavor to express it analytically with an adequate J–V model that does not implicitly or explicitly assume flat Fermi levels as does in the conventional one-diode model. We observed that the model recently introduced by Sandberg et al.[43] provides a good agreement with numerical simulations. It can reproduce the trend of $R_{p,photo}\phi$ with varied mobilities and light intensities (Figures S10 and S11, Supporting Information). Leveraging the Sandberg model, we derived the equation of $R_{p,photo}\phi$. The detailed derivation of $R_{p,photo}\phi$ can be found in Note 1 of Supporting Information and leads to

$$R_{p,photo}\phi = \frac{1}{qf_A}\frac{V_{bi} \times (1 + C_2)^{3/2}}{C_1 + C_2} \tag{2}$$

where f_A is the fraction of light that is absorbed, V_{bi} is the built-in voltage, the constant C_1 is given by

$$C_1 \propto \frac{k_B T}{qV_{bi}} \times \frac{k_{dir}\epsilon\epsilon_0}{q\mu}, \tag{3}$$

and the constant C_2 by

$$C_2 = \frac{Gk_{dir}d^4}{4\mu^2 V_{bi}^2} \tag{4}$$

Here, k_B is the Boltzmann constant, q is the elementary charge, T is the temperature of a device, k_{dir} is the direct recombination rate, ϵ is the relative permittivity of the absorber layer, ϵ_0 is the permittivity of the air, G is the generation rate, d is the thickness of the absorber layer. It is essential to highlight that the Sandberg model focuses solely on bimolecular recombination. However, as we mentioned previously, due to existence of electrons and holes injected from the electrode, bimolecular recombination can still scale linearly or quadratic with light intensity. The constant C_1 is the first-order recombination correction factor of J_{sc}, which is influenced by material parameters such as k_{dir}, μ, and ϵ and considers the part of bimolecular recombination that scales linearly with the average excess carrier density and thereby the light intensity. The constant C_2 denotes the second-order recombination correction, which is proportional to the generation rate G and affected by additional material parameters. When mobilities are sufficiently high to assume $C_2 \ll 1$ and $C_2 \ll C_1$, the $R_{p,photo}\phi$ is a function of material parameters ($R_{p,photo}\phi \approx V_{bi}/C_1$) and independent of light intensity. It is, hence, possible to extract information about material parameters from the $R_{p,photo}\phi$, since

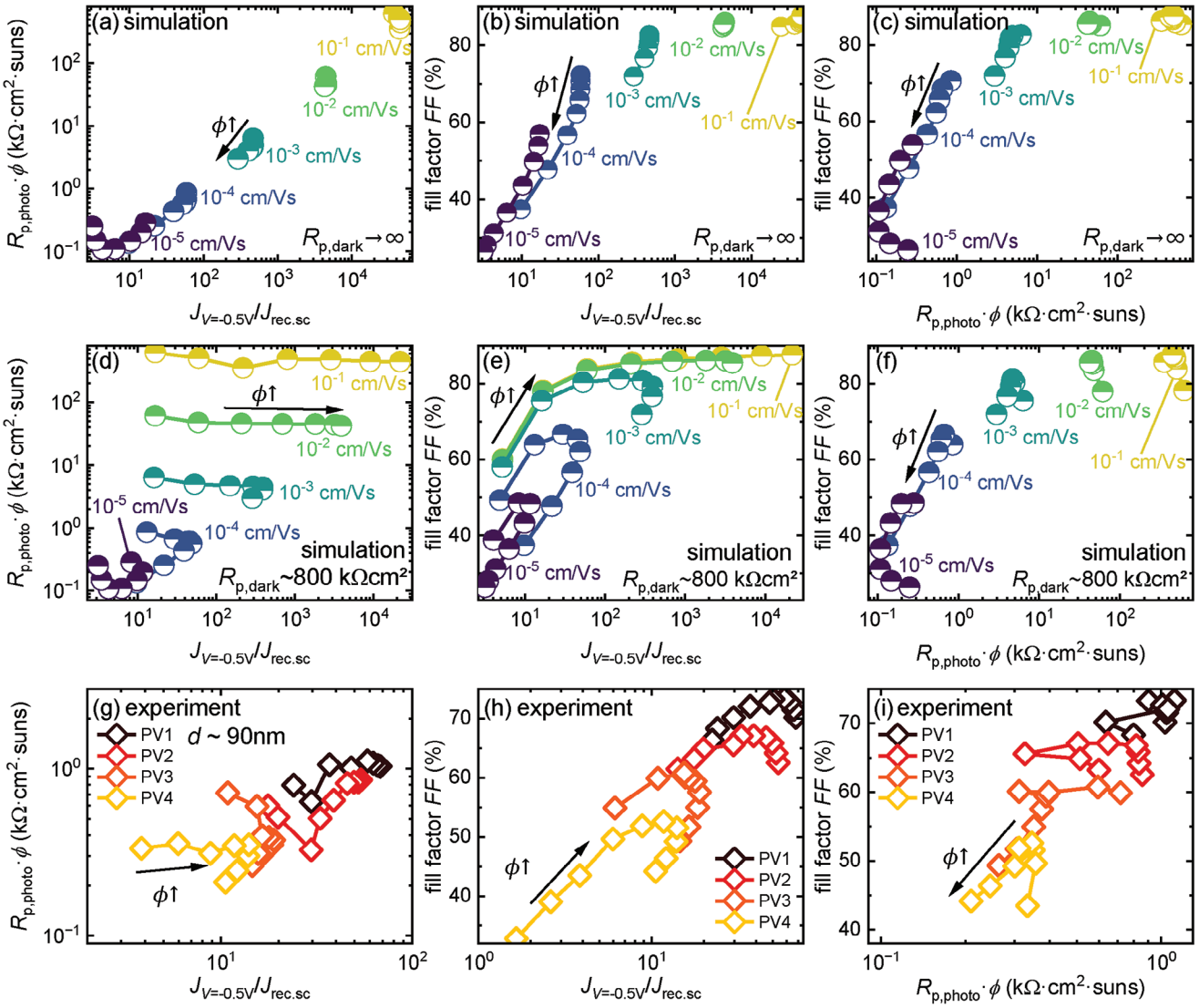

Figure 5. $R_{p,photo}\phi$, $J_{V=-0.5\,V}/J_{rec,sc}$, and *FF* from a–f) simulated and g–i) measured *JV* characteristics of varied light intensity. In simulations, the mobility of the active layer ranged from 10^{-1} to 10^{-5} cm^2 V^{-1} s^{-1} and the dark shunt resistance was set to a–c) 10^7 and d–f) 800 kΩ cm^2. Arrows indicate the variation in light intensity within the cell with same mobilities. PV1-4 has the identical cell stack and thickness to the active layer of PM6:Y6-1O:BO-4Cl, while the experimental conditions of the active layer were adjusted to change their charge transport properties. $R_{p,photo}$ was corrected with the $R_{p,total}$ at the lowest light intensity and, therefore, $R_{p,photo}$ of the lowest light intensity is not included in the plots. Higher $R_{p,photo}\phi$, $J_{V=-0.5\,V}/J_{rec,sc}$, and *FF* imply better charge extraction in the absorber layer.

$R_{p,photo}\phi \propto \mu/k_{dir}$. However, as the second-order recombination becomes dominant in the case of such as high ϕ or low μ, $R_{p,photo}\phi$ no longer remains constant across different light intensities and further simplification of $R_{p,photo}\phi$ is not possible. Nevertheless, the analytical expression of $R_{p,photo}\phi$ supports that this readily available observable contains information about material parameters and, consequently, allows us to quantify the charge collection efficiency of a solar cell.

In the following section, we use $R_{p,photo}\phi$ for analysis of the experimental data of PM6:Y6-1O:BO-4Cl cells and show how it can be interpreted based on drift-diffusion simulations. Here, we incorporated two additional observables in the *J*–*V* characteristics which represent charge recombination losses, each with a slightly different physical origin. One method is to determine the ratio of the generation current J_{gen} to the recombination current at short circuit $J_{rec,sc} = J_{gen} - J_{sc}$. Given the challenge of experimentally estimating J_{gen}, we replaced J_{gen} with the current density at a reverse bias of −0.5 V ($J_{V=-0.5\,V}$) and, therefore, $J_{rec,sc} = J_{V=-0.5\,V} - J_{sc}$. A higher ratio $J_{V=-0.5\,V}/J_{rec,sc}$ indicates smaller recombination losses at short circuit, while the leakage current due to $R_{p,dark}$ can play a key role in this ratio. Additionally, the fill factor *FF* is used for evaluating the voltage dependence and overall charge extraction efficiency. It is worth noting that the three metrics – $R_{p,photo}\phi$, *FF*, and $J_{V=-0.5\,V}/J_{rec,sc}$ – are defined such that enhanced extraction of photogenerated charges at short-circuit correlates with higher values of all three metrics. **Figure 5**a–f shows the plots of the three FOMs as a function of the other based on the simulated *J*–*V* curves where the mobility and the light intensity

were varied. We performed the simulation under two scenarios: one case where $R_{p,dark}$ is assumed to be infinite (Figure 5a–c) and the other where $R_{p,dark}$ assumes a more realistic value of 800 kΩ cm^2 (Figure 5d–f). Within each sub-figure, color variation represents the changes in mobility, while several points of the same color indicate variation in light intensity ranging from 10^{-4} to 1 sun.

First, we investigate the ideal case where there is no leakage current attributed to $R_{p,dark}$. As the color of the points in Figure 5a-c transitions from dark purple to yellow, both $R_{p,photo}\phi$ and $J_{V=-0.5\,V}/J_{rec,sc}$ increase, while *FF* increases as well but eventually saturates at its maximum point. This shows that higher values of $R_{p,photo}\phi$, $J_{V=-0.5\,V}/J_{rec,sc}$, and *FF* correspond to higher mobilities or better charge collection efficiency. By plotting one FOM as a function of another rather than as that of light intensities, we can clearly see the correlation between each pair of two FOMs, highlighting their dependence on mobilities or light intensities. In the case of an infinitely large dark shunt resistance, the three FOMs are approximately proportional to mobilities, causing the series of points with the same color to shift toward upward-right direction as mobilities increase. Examining the light intensity dependence, we observe that for solar cells with mobilities higher than 10^{-2} cm^2 V^{-1} s^{-1}, the circle points with the same color overlap (Figure 5a–c), indicating the constant $R_{p,photo}\phi$ and $J_{V=-0.5\,V}/J_{rec,sc}$ over different light intensities. According to the Sandberg model and the earlier discussion on constant $R_{p,photo}\phi$, this suggests that bimolecular recombination scales linearly with the average excess carrier density at short-circuit. For mobilities lower than 10^{-2} cm^2 V^{-1} s^{-1}, light intensity becomes more significant in determining the charge extraction efficiency that $R_{p,photo}\phi$, $J_{V=-0.5\,V}/J_{rec,sc}$, and *FF* started to decrease at higher light intensity, changing the plot shape from a dot of superimposed points to a straight line on a double-logarithmic plot. The further decrease in $R_{p,photo}\phi$ and $J_{V=-0.5\,V}/J_{rec,sc}$ over light intensities, implying that the recombination loss at short-circuit is primarily due to the second-order bimolecular recombination involving both photogenerated electrons and holes, and the recombination limited by the photoshunt is getting more significant. Lastly, in Figure 5a, an interesting "hockey-stick" shape appears for the lowest mobility (10^{-5} cm^2 V^{-1} s^{-1}). This feature originates from the increase of $R_{p,photo}\phi$ at higher light intensity, while $J_{V=-0.5\,V}/J_{rec,sc}$ decreases and is caused by the influence of low mobilities on series resistance, as previously discussed.

Since in non-idealized situations, the leakage current from the $R_{p,dark}$ affects the performance of a solar cell, simulations including a realistic value of the $R_{p,dark}$ for a 100nm-thick cell were performed. (Figure 5d–f) The influence of the $R_{p,dark}$ on overall performance of a solar cell is most prominent under low-light conditions, where $J_{rec,sc}$ is significantly affected by the leakage current $R_{p,dark}/V$ and, leading to a drop in *FF*. Comparing Figure 5a,d, the influence of $R_{p,dark}$ on $J_{rec,sc}$ is highlighted by the emergence of horizontal lines for data points representing the same mobility but different light intensities. For the device with high mobilities, $J_{V=-0.5\,V}/J_{rec,sc}$ continuously decreases as light intensity decreases, while $R_{p,photo}\phi$ remains approximately constant. Since $R_{p,photo}$ already excluded the effect of $R_{p,dark}$, including $R_{p,dark}$ in the simulation does not significantly changes the value of $R_{p,photo}\phi$, suggesting that it represents charge collection efficiency dependent on increased excess charge carrier densities under illumination. Moreover, significant leakage currents through pinholes in the device result in a decrease of *FF* at low light intensities and the "upside-down U" shape of the plot observed in Figure 5e. Since the leakage current from dark shunt at low light intensities is significantly dominating $J_{rec,sc}$ compared to transport-limited recombination current, $R_{p,dark}$ should be well-controlled, especially for higher mobility devices, in order to achieve high efficiency. On the other hand, at higher light intensity, plots with a realistic $R_{p,dark}$ resemble those with an infinite $R_{p,dark}$, implying that the $R_{p,dark}$ is no longer a dominant loss mechanism whereas poor charge transport dependent on light intensity plays a key role in determining the device's performance.

We performed the *J*–*V* characteristic measurements with a white LED lamp for organic solar cells with the active layer of PM6:Y6-1O:BO-4Cl, fabricated with different combinations of process parameters but maintaining a consistent thickness of ≈90 nm. Since each solar cell was produced with an identical stack design, its overall performance hinges on the charge transport property of the active layer. We use the results shown in Figure 5g–i to analyze charge extraction efficiency depending on their charge transport properties. All four devices inevitably suffer from existence of external resistances, demonstrated by "upside-down U" shape plots in Figure 5h. Still, the PV1 shows the highest value of $R_{p,photo}\phi$, $J_{V=-0.5\,V}/J_{rec,sc}$, and *FF*, indicating it has the most efficient charge transport property among four devices. The $R_{p,photo}\phi$ of the PV1 and the PV2 is scattering at low-light regime due to the unstable signal over voltages but has an almost constant value at higher light intensities. Based on the simulation result and the Sandberg model, the independence of $R_{p,photo}\phi$ on light intensity indicates that the recombination rate scales linearly with light intensity. Conversely, $R_{p,photo}\phi$ of PV3 and PV4 remains approximately constant with increasing light intensity, after which it decreases. The decrease of $R_{p,photo}\phi$ at higher light intensities suggests that the recombination mechanism where photogenerated electrons and holes take part is dominating the cell. The inefficient charge transport is additionally emphasized in decrease of $J_{V=-0.5\,V}/J_{rec,sc}$ at higher light intensities.

3. Conclusion

In organic solar cells, it is universally observed that under illumination, recombination current at low voltages is limited by an apparent shunt-like current that we refer to as photoshunt. In this work, we propose using photoshunt as an indicator of charge collection losses at short circuit. The photoshunt is strongly influenced by the light intensity due to the inherent dependence of charge carrier densities on the generation rate and thereby the light intensity. The strong relationship between photoshunt and light intensity leads us to investigate the product $R_{p,photo}\phi$ as a new figure of merit for assessing charge collection losses at short-circuit. We explore the impact of charge carrier mobility and light intensity on $R_{p,photo}\phi$, based on drift-diffusion simulations and an analytical model. As charge carrier mobilities increase, $R_{p,photo}\phi$ increases, as well as $J_{V=-0.5\,V}/J_{rec,sc}$ and *FF*. This increase in all three observables reflects enhanced charge extraction efficiency at short circuit. However, once $R_{p,dark}$ is included, $J_{V=-0.5\,V}/J_{rec,sc}$ and *FF* drop-down at low light intensities and no

longer share the same trend with $R_{p,photo}\phi$. In other words, unlike $J_{V=-0.5\,V}/J_{rec,sc}$, and *FF*, $R_{p,photo}\phi$ allows us to rule out the influence of external resistance $R_{p,dark}$ in understanding recombination losses and, thereby providing insight into charge carrier mobilities. When the impact of external resistance cannot be neglected, all three metrics are useful for comprehensively understanding recombination losses at short circuit. In this context, we present an analytical framework that incorporates three figures of merit $R_{p,photo}\phi$, $J_{V=-0.5\,V}/J_{rec,sc}$, and *FF*. By comparing the experimental results of organic solar cells with different process parameters, the proposed method of plotting three FOMs allows us to quantify the charge transport properties of organic bulk layers.

The discussion within the present study focuses entirely on the interpretation of the data within the framework of charge carrier recombination and transport. However, in excitonic solar cells, also alternative interpretations for deviations from the superposition principle are possible. Field- or voltage-dependent geminate recombination can lead to a voltage-dependent generation of free charge carriers and therefore also a voltage-dependent photocurrent in the absence of significant transport losses. As the resulting photoshunt resistance would also scale inversely with light intensity, the analysis of the current-voltage curve alone would not suffice to discriminate between geminate and non-geminate recombination effects. Thus, future work on understanding the photoshunt will have to involve methods that discriminate between those effects based on the different timescales of geminate and non-geminate recombination[44,45] or alternatively the different degrees of luminescence efficiency.[38,46]

Supporting Information

Supporting Information is available from the Wiley Online Library or from the author.

Acknowledgements

The authors acknowledge funding by the Helmholtz Association via the POF IV funding as well as via the SolarTap project. The authors further thank the Ministry of Economic Affairs, Industry, Climate Action and Energy of the State of North Rhine-Westphalia for funding via the ENFA ("Entwicklung effizienter ternärer NFA-basierter organischer Photovoltaik durch Machine-Learning Methoden") project.

Open access funding enabled and organized by Projekt DEAL.

Conflict of Interest

The authors declare no conflict of interest.

Data Availability Statement

The data that used in the main text are available in https://zenodo.org/records/12624861. Further information and data are available from the authors upon request.

Keywords

mobility, recombination losses, resistive losses, transport

Received: July 17, 2024
Revised: September 16, 2024
Published online: October 3, 2024

[1] Y. Cui, Y. Xu, H. Yao, P. Bi, L. Hong, J. Zhang, Y. Zu, T. Zhang, J. Qin, J. Ren, Z. Chen, C. He, X. Hao, Z. Wei, J. Hou, *Adv. Mater.* **2021**, *33*, 2102420.
[2] W. Gao, F. Qi, Z. Peng, F. R. Lin, K. Jiang, C. Zhong, W. Kaminsky, Z. Guan, C.-S. Lee, T. J. Marks, H. Ade, A. K. Y. Jen, *Adv. Mater.* **2022**, *34*, 2202089.
[3] C. He, Y. Pan, Y. Ouyang, Q. Shen, Y. Gao, K. Yan, J. Fang, Y. Chen, C.-Q. Ma, J. Min, C. Zhang, L. Zuo, H. Chen, *Energy Environ. Sci.* **2022**, *15*, 2537.
[4] L. Zhu, M. Zhang, J. Xu, C. Li, J. Yan, G. Zhou, W. Zhong, T. Hao, J. Song, X. Xue, Z. Zhou, R. Zeng, H. Zhu, C.-C. Chen, R. C. I. MacKenzie, Y. Zou, J. Nelson, Y. Zhang, Y. Sun, F. Liu, *Nat. Mater.* **2022**, *21*, 656.
[5] C. Han, J. Wang, S. Zhang, L. Chen, F. Bi, J. Wang, C. Yang, P. Wang, Y. Li, X. Bao, *Adv. Mater.* **2023**, *35*, 2208986.
[6] M. Green, E. Dunlop, J. Hohl-Ebinger, M. Yoshita, N. Kopidakis, X. Hao, *Prog. Photovoltaics* **2021**, *29*, 3.
[7] C. Liu, Y. Yang, H. Chen, J. Xu, A. Liu, A. S. R. Bati, H. Zhu, L. Grater, S. S. Hadke, C. Huang, V. K. Sangwan, T. Cai, D. Shin, L. X. Chen, M. C. Hersam, C. A. Mirkin, B. Chen, M. G. Kanatzidis, E. H. Sargent, *Science* **2023**, *382*, 810.
[8] H. Lin, M. Yang, X. Ru, G. Wang, S. Yin, F. Peng, C. Hong, M. Qu, J. Lu, L. Fang, C. Han, P. Procel, O. Isabella, P. Gao, Z. Li, X. Xu, *Nat. Energy* **2023**, *8*, 789.
[9] F. F. Stelzl, U. Würfel, *Phys. Rev. B* **2012**, *86*, 075315.
[10] U. Wurfel, D. Neher, A. Spies, S. Albrecht, *Nat. Commun.* **2015**, *6*, 6951.
[11] D. Cheyns, J. Poortmans, P. Heremans, C. Deibel, S. Verlaak, B. P. Rand, J. Genoe, *Phys. Rev. B* **2008**, *77*, 165332.
[12] M. Saladina, C. Deibel, *arXiv:2404.06190* **2024**.
[13] D. Neher, J. Kniepert, A. Elimelech, L. J. A. Koster, *Sci. Rep.* **2016**, *6*, 24861.
[14] M. C. Heiber, T. Okubo, S.-J. Ko, B. R. Luginbuhl, N. A. Ran, M. Wang, H. Wang, M. A. Uddin, H. Y. Woo, G. C. Bazan, T.-Q. Nguyen, *Energy Environ. Sci.* **2018**, *11*, 3019.
[15] L. J. A. Koster, V. D. Mihailetchi, H. Xie, P. W. M. Blom, *Appl. Phys. Lett.* **2005**, *87*, 203502.
[16] L. J. A. Koster, M. Kemerink, M. M. Wienk, K. Maturová, R. A. J. Janssen, *Adv. Mater.* **2011**, *23*, 1670.
[17] C. Sun, F. Pan, H. Bin, J. Zhang, L. Xue, B. Qiu, Z. Wei, Z.-G. Zhang, Y. Li, *Nat. Commun.* **2018**, *9*, 743.
[18] B. Guo, W. Li, X. Guo, X. Meng, W. Ma, M. Zhang, Y. Li, *Adv. Mater.* **2017**, *29*, 1702291.
[19] M. Lenes, M. Morana, C. J. Brabec, P. W. M. Blom, *Adv. Funct. Mater.* **2009**, *19*, 1106.
[20] Y. Lin, F. Zhao, Y. Wu, K. Chen, Y. Xia, G. Li, S. K. K. Prasad, J. Zhu, L. Huo, H. Bin, Z.-G. Zhang, X. Guo, M. Zhang, Y. Sun, F. Gao, Z. Wei, W. Ma, C. Wang, J. Hodgkiss, Z. Bo, O. Inganäs, Y. Li, X. Zhan, *Adv. Mater.* **2017**, *29*, 1604155.
[21] F. Zhao, S. Dai, Y. Wu, Q. Zhang, J. Wang, L. Jiang, Q. Ling, Z. Wei, W. Ma, W. You, C. Wang, X. Zhan, *Adv. Mater.* **2017**, *29*, 1700144.
[22] I. Riedel, J. Parisi, V. Dyakonov, L. Lutsen, D. Vanderzande, J. C. Hummelen, *Adv. Funct. Mater.* **2004**, *14*, 38.
[23] L. Yang, S. Zhang, C. He, J. Zhang, H. Yao, Y. Yang, Y. Zhang, W. Zhao, J. Hou, *J. Am. Chem. Soc.* **2017**, *139*, 1958.
[24] S. Guan, Y. Li, C. Xu, N. Yin, C. Xu, C. Wang, M. Wang, Y. Xu, Q. Chen, D. Wang, L. Zuo, H. Chen, *Adv. Mater.* **2024**, *36*, 2400342.
[25] T. Zhang, C. An, Y. Cui, J. Zhang, P. Bi, C. Yang, S. Zhang, J. Hou, *Adv. Mater.* **2022**, *34*, 2105803.
[26] A. Paulke, S. D. Stranks, J. Kniepert, J. Kurpiers, C. M. Wolff, N. Schön, H. J. Snaith, T. J. K. Brenner, D. Neher, *Appl. Phys. Lett.* **2016**, *108*, 113505.

[27] J. Kurpiers, T. Ferron, S. Roland, M. Jakoby, T. Thiede, F. Jaiser, S. Albrecht, S. Janietz, B. A. Collins, I. A. Howard, D. Neher, *Nat. Commun.* **2018**, *9*, 2038.
[28] J. Kniepert, M. Schubert, J. C. Blakesley, D. Neher, *J. Phys. Chem. Lett.* **2011**, *2*, 700.
[29] S. Karuthedath, A. Melianas, Z. Kan, V. Pranculis, M. Wohlfahrt, J. I. Khan, J. Gorenflot, Y. Xia, O. Inganäs, V. Gulbinas, M. Kemerink, F. Laquai, *J. Mater. Chem. A* **2018**, *6*, 7428.
[30] S. J. Robinson, A. G. Aberle, M. A. Green, *J. Appl. Phys.* **1994**, *76*, 7920.
[31] D. Wang, G. Q. Zhou, Y. H. Li, K. R. Yan, L. L. Zhan, H. M. Zhu, X. H. Lu, H. Z. Chen, C. Z. Li, *Adv. Funct. Mater.* **2022**, *32*, 2107827.
[32] L. Meng, Y. Zhang, X. Wan, C. Li, X. Zhang, Y. Wang, X. Ke, Z. Xiao, L. Ding, R. Xia, H.-L. Yip, Y. Cao, Y. Chen, *Science* **2018**, *361*, 1094.
[33] D. Lubke, P. Hartnagel, M. Hulsbeck, T. Kirchartz, *ACS Mater. Au* **2023**, *3*, 215.
[34] C. Y. Liao, Y. T. Hsiao, K. W. Tsai, N. W. Teng, W. L. Li, J. L. Wu, J. C. Kao, C. C. Lee, C. M. Yang, H. S. Tan, K. H. Chung, Y. M. Chang, *Sol. RRL* **2021**, *5*, 2000749.
[35] D. Lübke, P. Hartnagel, J. Angona, T. Kirchartz, *Adv. Energy Mater.* **2021**, *11*, 2101474.
[36] D. Grabowski, Z. F. Liu, G. Schope, U. Rau, T. Kirchartz, *Sol. RRL* **2022**, *6*, 2200507.
[37] O. Breitenstein, *IEEE J. Photovoltaics* **2014**, *4*, 899.
[38] M. Pranav, T. Hultzsch, A. Musiienko, B. Sun, A. Shukla, F. Jaiser, S. Shoaee, D. Neher, *APL Mater.* **2023**, *11*, 061111.
[39] M. Pranav, A. Shukla, D. Moser, J. Rumeney, W. Liu, R. Wang, B. Sun, S. Smeets, N. Tokmoldin, Y. Cao, G. He, T. Beitz, F. Jaiser, T. Hultzsch, S. Shoaee, W. Maes, L. Lüer, C. Brabec, K. Vandewal, D. Andrienko, S. Ludwigs, D. Neher, *Energy Environ. Sci.* **2024**.
[40] G. F. A. Dibb, F. C. Jamieson, A. Maurano, J. Nelson, J. R. Durrant, *J. Phys. Chem. Lett.* **2013**, *4*, 803.
[41] C. G. Shuttle, R. Hamilton, B. C. O'Regan, J. Nelson, J. R. Durrant, *Proc. Natl. Acad. Sci.* **2010**, *107*, 16448.
[42] U. Wurfel, L. Perdigon-Toro, J. Kurpiers, C. M. Wolff, P. Caprioglio, J. J. Rech, J. S. Zhu, X. W. Zhan, W. You, S. Shoaee, D. Neher, M. Stolterfoht, *J. Phys. Chem. Lett.* **2019**, *10*, 3473.
[43] O. J. Sandberg, A. Armin, *PRX Energy* **2024**, *3*, 023008.
[44] U. Würfel, M. Unmüssig, *Sol RRL* **2018**, *2*, 1800229.
[45] B. Gerber, N. Tokmoldin, O. J. Sandberg, E. Sağlamkaya, B. Sun, S. Shoaee, D. Neher, *Sol. RRL* **2024**, *8*, 2400083.
[46] K. Tvingstedt, K. Vandewal, F. Zhang, O. Inganäs, *J. Phys. Chem. C* **2010**, *114*, 21824.